

# Fundamental limits on the rate of bacterial cell division

<sup>3</sup> Nathan M. Belliveau<sup>†, 1</sup>, Griffin Chure<sup>†, 2, 3</sup>, Christina L. Hueschen<sup>4</sup>, Hernan G.  
<sup>4</sup> Garcia<sup>5</sup>, Jané Kondev<sup>6</sup>, Daniel S. Fisher<sup>7</sup>, Julie Theriot<sup>1, 2, 8</sup>, Rob Phillips<sup>1, 2, 9, \*</sup>

\*For correspondence:

<sup>†</sup>These authors contributed equally to this work

<sup>5</sup> Department of Biology, University of Washington, Seattle, WA, USA; <sup>2</sup>Division of  
<sup>6</sup> Biology and Biological Engineering, California Institute of Technology, Pasadena, CA,  
<sup>7</sup> USA; <sup>3</sup>Department of Applied Physics, California Institute of Technology, Pasadena, CA,  
<sup>8</sup> USA; <sup>4</sup>Department of Chemical Engineering, Stanford University, Stanford, CA, USA;  
<sup>9</sup> Department of Molecular Cell Biology and Department of Physics, University of  
<sup>10</sup> California Berkeley, Berkeley, CA, USA; <sup>6</sup>Department of Physics, Brandeis University,  
<sup>11</sup> Waltham, MA, USA; <sup>7</sup>Department of Applied Physics, Stanford University, Stanford, CA,  
<sup>12</sup> USA; <sup>8</sup>Allen Institute for Cell Science, Seattle, WA, USA; <sup>9</sup>Department of Physics,  
<sup>13</sup> California Institute of Technology, Pasadena, CA, USA; \* Contributed equally

14

---

## 15 Abstract

16

---

## 17 Introduction

18 The range of bacterial growth rates can be enormous. In natural environments, some microbial  
<sup>19</sup> organisms might double only once per year, whereas in comfortable laboratory conditions growth  
<sup>20</sup> can be rapid with several divisions per hour. This remarkable diversity illustrates the intimate re-  
<sup>21</sup> lationship between environmental conditions and the rates at which cells convert nutrients into  
<sup>22</sup> new cellular material. This relationship between the environment and cellular growth rate has re-  
<sup>23</sup> mained a major topic of inquiry in bacterial physiology for over a century (*Jun et al., 2018*). In 1958,  
<sup>24</sup> Schaecter, Malløe, and Kjeldgaard reported the discovery of a logarithmic relationship between  
<sup>25</sup> the total cellular protein content and the cellular growth rate, revealing a fundamental rela-  
<sup>26</sup> tionship between the environment and the composition of the intracellular milieu (*Schaechter et al.,*  
<sup>27</sup> *1958*).

28 Over the past decade, a remarkable body of work has reexamined this relationship with single-  
<sup>29</sup> cell and single-protein resolution using modern methods of video microscopy (*Si et al., 2017; Har-*  
<sup>30</sup> *riss and Theriot, 2018*) and through advances in mass spectrometry and sequencing technologies  
<sup>31</sup> (*Schmidt et al., 2016; Li et al., 2014*). This has permitted quantitative insight into how bacteria like  
<sup>32</sup> *E. coli* allocate their cellular resources under nutrient-limitation, and following genomic and phar-  
<sup>33</sup> macological perturbations (*Scott et al., 2010; Hui et al., 2015; Basan et al., 2015*). This body of  
<sup>34</sup> experimental data places us in the auspicious position to explore how the abundance of essential  
<sup>35</sup> protein complexes are related to the growth rate of the population and interrogate what biological  
<sup>36</sup> processes may set the speed limit of bacterial growth.

37 In this work, we seek to leverage a collection of proteomic data sets of *Escherichia coli* across 31  
<sup>38</sup> growth conditions (*Valgepea et al., 2013; Li et al., 2014; Peebo et al., 2015; Hui et al., 2015; Schmidt*  
<sup>39</sup> *et al., 2016*) to quantitatively explore what biological processes may set the speed limit of bacterial  
<sup>40</sup> growth. Broadly speaking, we entertain several classes of hypotheses as are illustrated in *Figure 1*.  
<sup>41</sup> First, we consider potential limits on the transport of nutrients into the cell. We address this hy-

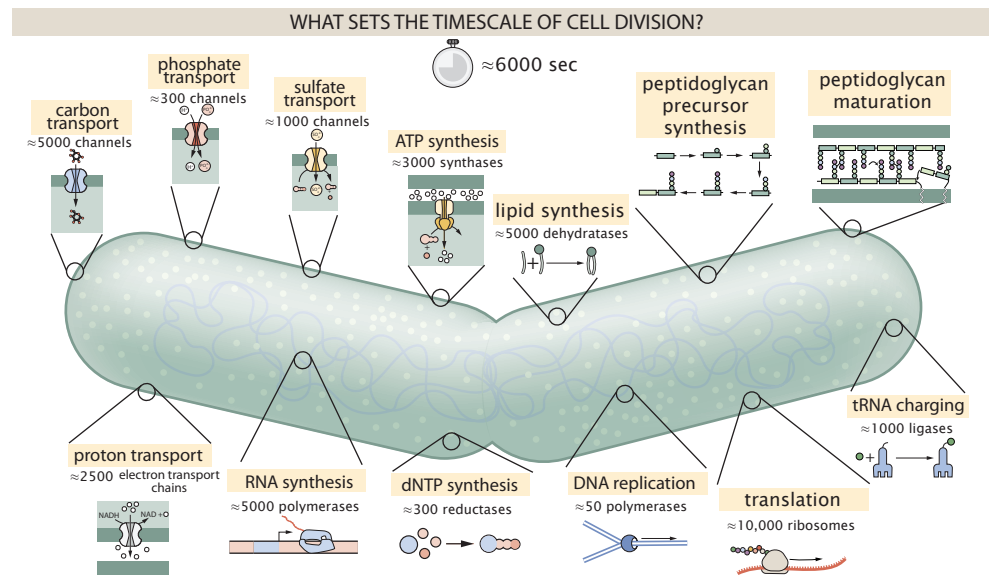


**Figure 1. Transport and synthesis processes necessary for cell division.** We consider an array of processes necessary for a cell to double its molecular components. Such processes include the transport of carbon across the cell membrane, the production of ATP, and fundamental processes of the central dogma namely RNA, DNA, and protein synthesis. A schematic of each synthetic or transport category is shown with an estimate of the rate per macromolecular complex. In this work, we consider a standard bacterial division time of  $\approx 6000$  sec.

42 pothesis by performing an order-of-magnitude estimate for how many carbon atoms needed to  
 43 facilitate this requirement given a 6000 second division time. As a second hypothesis, we consider  
 44 the possibility that there exists a fundamental limit on how quickly the cell can generate ATP. We ap-  
 45 proach this hypothesis from two angles, considering how many ATP synthase complexes must be  
 46 needed to churn out enough ATP to power protein translation followed by an estimation of how  
 47 many electron transport complexes must be present to maintain the proton motive force. Our  
 48 third and final class of hypotheses centers on the synthesis of a variety of biomolecules. Our focus  
 49 is primarily on the stages of the central dogma as we estimate the number of protein complexes  
 50 needed for DNA replication, transcription, and protein translation.

51 With estimates in hand for each of these processes, we turn to our collection of data sets to  
 52 assess the accuracy of our estimates. In broad terms, we find that the majority of our estimates are  
 53 in line with experimental observations, with protein copy numbers apparently well-tuned for the  
 54 task of cell doubling. This allows us to systematically scratch off the hypotheses diagrammed in **Fig-**  
**55 ure 1** as setting possible speed limits. Ultimately, we find that protein translation (particularly the  
 56 generation of new ribosomes) acts as 1) a rate limiting step for the *fastest* bacterial division, and 2)  
 57 the major determinant of bacterial growth across all nutrient conditions we have considered under  
 58 steady state, exponential growth. This perspective is in line with the linear correlation observed  
 59 between growth rate and ribosomal content (usually quantified through the ratio of RNA to pro-  
 60 tein) for fast growing cells (*Scott et al., 2010*), but suggests a more prominent role for ribosomes  
 61 in setting the doubling time across all conditions of nutrient limitation. Here we again leverage the  
 62 quantitative nature of this data set and present a quantitative model of the relationship between  
 63 the fraction of the proteome devoted to ribosomes and the speed limit of translation, revealing  
 64 a fundamental tradeoff between the translation capacity of the ribosome pool and the maximal  
 65 growth rate.

**66 Nutrient Transport**

67 In order to build new cellular mass, the molecular and elemental building blocks must be scav-  
 68 enged from the environment in different forms. Carbon, for example, is acquired via the transport  
 69 of carbohydrates and sugar alcohols with some carbon sources receiving preferential treatment  
 70 in their consumption (*Monod, 1947*). Phosphorus, sulfur, and nitrogen, on the other hand, are  
 71 harvested primarily in the forms of inorganic salts, namely phosphate, sulfate, and ammonia (*Jun*  
 72 *et al., 2018; Assentoft et al., 2016; Stasi et al., 2019; Antonenko et al., 1997; Rosenberg et al., 1977;*  
 73 *Willsky et al., 1973*). All of these compounds have different permeabilities across the cell mem-  
 74 brane and most require some energetic investment either via ATP hydrolysis or through the pro-  
 75 ton electrochemical gradient to bring the material across the hydrophobic cell membrane. Given  
 76 the diversity of biological transport mechanisms and the vast number of inputs needed to build a  
 77 cell, we begin by considering transport of elemental requirements as a possible rate-limiting step  
 78 of bacterial cell division.

79 The elemental composition of *E. coli* has received much quantitative attention over the past  
 80 half century (*Neidhardt et al., 1991; Taymaz-Nikerel et al., 2010; Heldal et al., 1985; Bauer and Ziv,*  
 81 *1976*), providing us with a starting point for estimating the copy numbers of various transporters.  
 82 While there is some variability in the exact elemental percentages (with different uncertainties), we  
 83 can estimate that the dry mass of a typical *E. coli* cell is  $\approx 45\%$  carbon (BNID: 100649, *Milo et al.*  
 84 (*2010*)),  $\approx 15\%$  nitrogen (BNID: 106666, *Milo et al. (2010)*),  $\approx 3\%$  phosphorus (BNID: 100653, *Milo*  
 85 *et al. (2010)*), and  $1\%$  sulfur (BNID: 100655, *Milo et al. (2010)*). In the coming paragraphs, we will  
 86 examine how many transporters and/or channels must be present to maintain these elemental  
 87 compositions with a moderate doubling time of 6,000 s.

**88 Carbon Transport**

89 We begin with the most abundant element by mass, carbon. Using  $\approx 0.3$  pg as the typical *E. coli*  
 90 dry mass (BNID: 103904, *Milo et al. (2010)*), we estimate that  $\approx 10^{10}$  carbon atoms must be brought  
 91 into the cell in order to double all of the carbon-containing molecules (*Figure 2(A, top)*). Typical  
 92 laboratory growth conditions, such as those explored in the aforementioned proteomic data sets,  
 93 provide carbon as single class of sugar such as glucose, galactose, or xylose to name a few. *E.*  
 94 *coli* has evolved myriad mechanisms by which these sugars can be transported across the cell  
 95 membrane. One such mechanism of transport is via the PTS system which is a highly modular  
 96 system capable of transporting a diverse range of sugars (*Escalante et al., 2012*). The glucose-  
 97 specific component of this system transports  $\approx 200$  glucose molecules per second per channel  
 98 (BNID: 114686, *Milo et al. (2010)*). Making the assumption that this is a typical sugar transport rate,  
 99 coupled with the need to transport  $10^{10}$  carbon atoms, we arrive at the conclusion that on the  
 100 order of 1,000 transporters must be expressed in order to bring in enough carbon atoms to divide  
 101 in 6,000 s, diagrammed in the top panel of *Figure 2(A)*. This estimate, along with the observed  
 102 average number of carbohydrate transporters present in the proteomic data sets (*Schmidt et al.,*  
 103 *2016; Peebo et al., 2015; Valgepea et al., 2013; Li et al., 2014*), is shown in *Figure 2(A)*. While we  
 104 estimate 1,000 transporters are needed, the data reveals that at a division time of  $\approx 6,000$  s there is  
 105 nearly a ten-fold excess of transporters. Furthermore, the data illustrates that the average number  
 106 of carbohydrate transporters present is largely-growth rate independent.

107 The estimate presented in *Figure 2(A)* neglects any specifics of the regulation of carbon trans-  
 108 port system and presents a data-averaged view of how many carbohydrate transporters are present  
 109 on average. Using the diverse array of growth conditions explored in the proteomic data sets,  
 110 we can explore how individual carbon transport systems depend on the population growth rate.  
 111 In *Figure 2(B)*, we show the total number of carbohydrate transporters specific to different car-  
 112 bon sources. A striking observation, shown in the top-left plot of *Figure 2(B)*, is the constancy  
 113 in the expression of the glucose-specific transport systems (the PtsG enzyme of the PTS system  
 114 and the glucose-transporting ManXYZ complex). Additionally, we note that the total number of  
 115 glucose-specific transporters is tightly distributed  $\approx 10^4$  per cell, an order of magnitude beyond

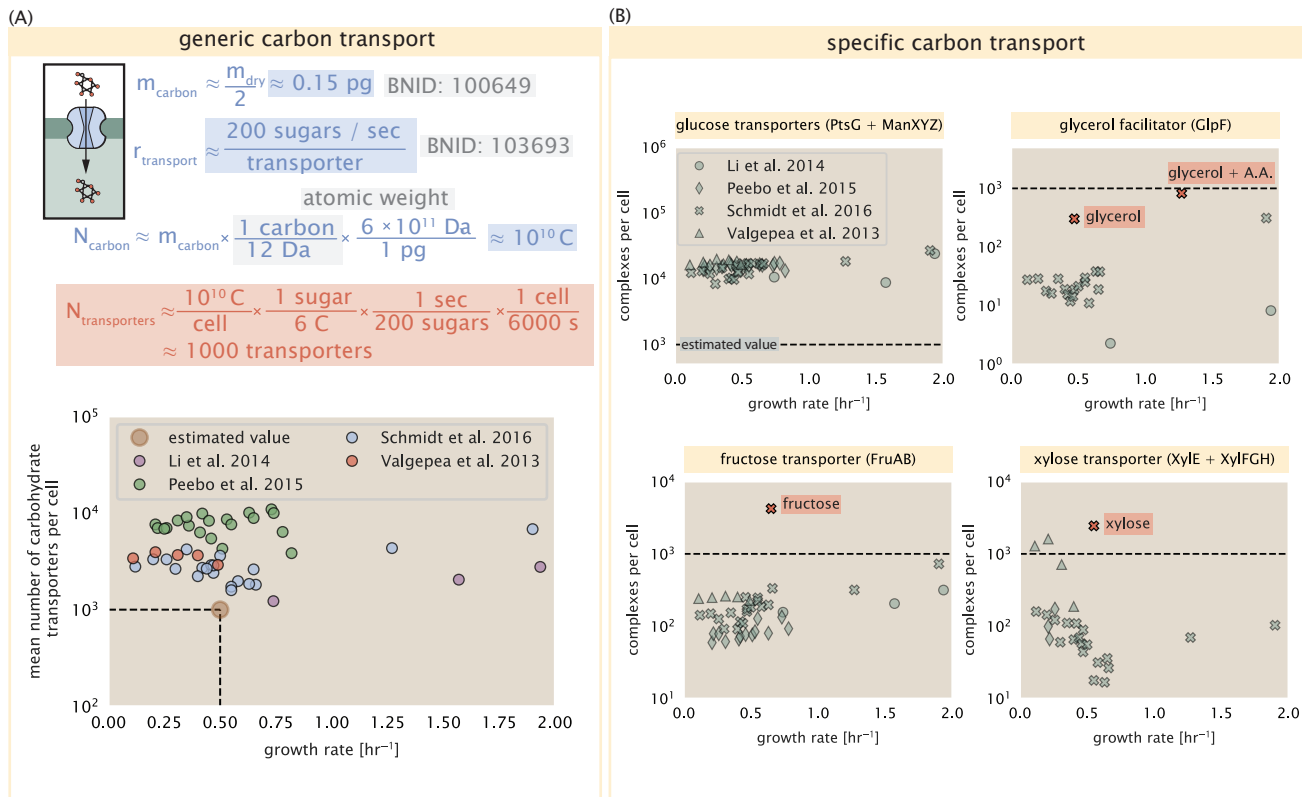


**Figure 2. The abundance of carbon transport systems across growth rates.** (A) A simple estimate for the minimum number of generic carbohydrate transport systems (top) assumes  $\approx 10^{10}$  C are needed to complete division, each transported sugar contains  $\approx 6$  C, and each transporter conducts sugar molecules at a rate of  $\approx 200$  per second. Bottom plot shows the estimated number of transporters needed at a growth rate of  $\approx 0.5$  per hr (light-brown point and dashed lines). Colored points correspond to the mean number of carbohydrate transporters for different growth conditions across different published datasets. (B) The abundance of various specific carbon transport systems plotted as a function of the population growth rate. Red points and red-highlighted text indicate conditions in which the only source of carbon in the growth medium induces expression of the transport system.

116 the estimate shown in **Figure 2(A)**. This illustrates that *E. coli* maintains a substantial number of  
 117 complexes present for transporting glucose which is known to be the preferential carbon source  
 118 (**Monod, 1947; Liu et al., 2005; Aidelberg et al., 2014**).

119 It is now understood that a large number of metabolic operons are regulated with dual-input  
 120 logic gates that are only expressed when glucose concentrations are low (mediated by cyclic-AMP  
 121 receptor protein CRP) and the concentration of other carbon sources are elevated (**Gama-Castro**  
 122 **et al., 2016; Zhang et al., 2014b**). A famed example of such dual-input regulatory logic is in the regu-  
 123 lation of the *lac* operon which is only natively activated in the absence of glucose and the presence  
 124 of allolactose, an intermediate in lactose metabolism (**Jacob and Monod, 1961**), though we now  
 125 know of many other such examples (**Ireland et al., 2020; Gama-Castro et al., 2016; Belliveau et al.,**  
 126 **2018**). This illustrates that once glucose is depleted from the environment, cells have a means to  
 127 dramatically increase the abundance of the specific transporter needed to digest the next sugar  
 128 that is present. Several examples of induced expression of a specific carbon-source transporters  
 129 are shown in **Figure 2(B)**. Points colored in red (labeled by red text-boxes) correspond to growth  
 130 conditions in which the specific carbon source (glycerol, xylose, or fructose) is present. These plots  
 131 show that, in the absence of the particular carbon source, expression of the transporters is main-  
 132 tained on the order of  $\sim 10^2$  per cell. However, when induced, the transporters become highly-  
 133 expressed and are present on the order of  $\sim 10^4$  per cell, which exceeds the generic estimate given  
 134 in **Figure 2(A)**. Together, this generic estimation and the specific examples of induced expression  
 135 suggest that transport of carbon across the cell membrane, while critical for growth, is not the  
 136 rate-limiting step of cell division.

137 In the context of speeding up growth, one additional limitation is the fact that the cell's inner  
 138 membrane is occupied by a multitude of other membrane proteins. Considering a rule-of-thumb  
 139 for the surface area of *E. coli* of about  $6 \mu\text{m}^2$  (BNID: 101792, **Milo et al. (2010)**), we expect an areal  
 140 density for 1,000 transporters to be approximately 200 transporters/ $\mu\text{m}^2$ . For a glucose trans-  
 141 porter occupying about  $50 \text{ nm}^2/\text{dimer}$ , this amounts to about only 1 percent of the total inner  
 142 membrane (**Szenk et al., 2017**). In addition, bacterial cell membranes typically have densities of  
 143  $10^5$  proteins/ $\mu\text{m}^2$  (**Phillips, 2018**), implying that the cell could accommodate more transporters if  
 144 it were rate limiting.

### 145 **Phosphorus and Sulfur Transport**

146 We now turn our attention towards other essential elements, namely phosphorus and sulfur. Phos-  
 147 phorus is critical to the cellular energy economy in the form of high-energy phosphodiester bonds  
 148 making up DNA, RNA, and the NTP energy pool as well as playing a critical role in the post-translational  
 149 modification of proteins and defining the polar-heads of lipids. In total, phosphorus makes up  
 150  $\approx 3\%$  of the cellular dry mass which in typical experimental conditions is in the form of inorganic  
 151 phosphate. The cell membrane has remarkably low permeability to this highly-charged and critical  
 152 molecule, therefore requiring the expression of active transport systems. In *E. coli*, the proton elec-  
 153 trochemical gradient across the inner membrane is leveraged to transport inorganic phosphate  
 154 into the cell (**Rosenberg et al., 1977**). Proton-solute symporters are widespread in *E. coli* (**Ramos and**  
 155 **Kaback, 1977; Booth et al., 1979**) and can have rapid transport rates of 50 molecules per second  
 156 for sugars and other solutes (BNID: 103159; 111777, **Milo et al. (2010)**). In *E. coli* the PitA phosphate  
 157 transport system has been shown to very tightly coupled with the proton electrochemical gradient  
 158 with a 1:1 proton:phosphate stoichiometric ratio (**Harris et al., 2001; Feist et al., 2007**). Illustrated  
 159 in **Figure 3(A)**, we can estimate that  $\approx 300$  phosphate transporters are necessary to maintain an  
 160  $\approx 3\%$  dry mass with a 6,000 s division time. This estimate is again satisfied when we examine the  
 161 observed copy numbers of PitA in proteomic data sets (plot in **Figure 3(A)**). While our estimate is  
 162 very much in line with the observed numbers, we emphasize that this is likely a slight over estimate  
 163 of the number of transporters needed as there are other phosphorous scavenging systems, such  
 164 as the ATP-dependent phosphate transporter Pst system which we have neglected.

165 Satisfied that there are a sufficient number of phosphate transporters present in the cell, we

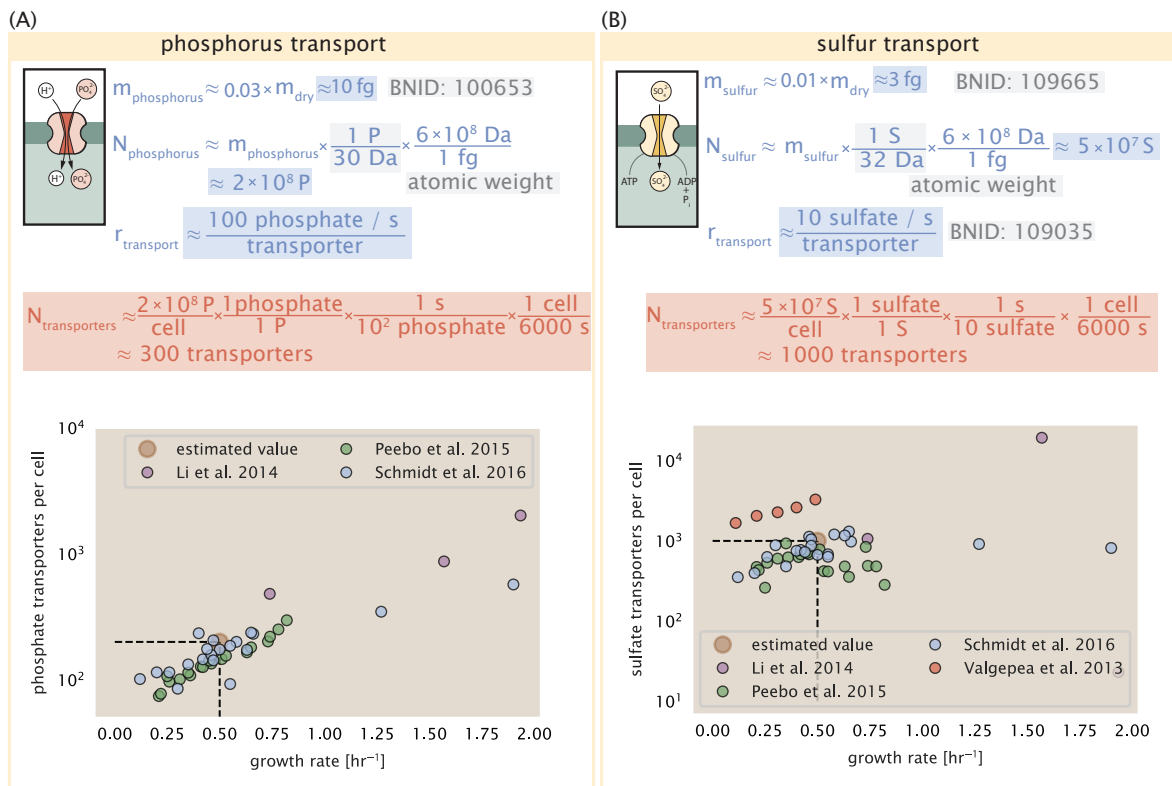


**Figure 3. Estimates and measurements of phosphate and sulfate transport systems as a function of growth rate.** (A) Estimate for the number of PitA phosphate transport systems needed to maintain a 3% phosphorus *E. coli* dry mass. Points in plot correspond to the total number of PitA transporters per cell. (B) Estimate of the number of CysUWA complexes necessary to maintain a 1% sulfur *E. coli* dry mass. Points in plot correspond to average number of CysUWA transporter complexes that can be formed given the transporter stoichiometry [CysA]<sub>2</sub>[CysU][CysW][Sbp/CysP].

now turn sulfur transport as another potentially rate limiting process. Similar to phosphate, sulfate is highly-charged and not particularly membrane permeable, requiring active transport. While there exists a H+/sulfate symporter in *E. coli*, it is in relatively low abundance and is not well characterized (Zhang et al., 2014a). Sulfate is predominantly acquired via the ATP-dependent ABC transporter CysUWA system which also plays an important role in selenium transport (Sekowska et al., 2000; Sirko et al., 1995). While specific kinetic details of this transport system are not readily available, generic ATP transport systems in prokaryotes are on the order of 1 to 10 molecules per second (BNID: 109035, Milo et al. (2010)). Combining this generic transport rate, measurement of sulfur comprising 1% of dry mass, and a 6,000 second division time yields an estimate of  $\approx 1000$  CysUWA complexes per cell (Figure 3(B)). Once again, this estimate is in notable agreement with proteomic data sets, suggesting that there are sufficient transporters present to acquire the necessary sulfur. In a similar spirit of our estimate of phosphorus transport, we emphasize that this is likely an overestimate of the number of necessary transporters as we have neglected other sulfur scavenging systems that are in lower abundance.

### 180 Nitrogen Transport

Finally, we turn to nitrogen transport as the last remaining transport system highlighted in Figure 1. Unlike phosphate, sulfate, and various sugar molecules, nitrogen in the form of ammonia can readily diffuse across the cell membrane and has a permeability on par with water ( $\approx 10^5$  nm/s, BNID: 110824 Milo et al. (2010)). In particularly nitrogen-poor conditions, *E. coli* expresses a transporter (AmtB) which appears to aid in nitrogen assimilation, though the mechanism and kinetic

186 details of transport is still a matter of debate (*van Heeswijk et al., 2013; Khademi et al., 2004*). Be-  
 187 yond ammonia, another plentiful source of nitrogen come in the form of glutamate, which has it's  
 188 own complex metabolism and scavenging pathways. However, nitrogen is plentiful in the growth  
 189 conditions examined in this work, permitting us to neglect nitrogen transport as a potential rate  
 190 limiting process in cell division.

## 191 Energy Production

192 While the transport of nutrients is required to build new cell mass, the metabolic pathways in-  
 193 volved in assimilation both consumes and generates energy in the form of NTPs. The high-energy  
 194 phosphodiester bonds of (primarily) ATP power a variety of cellular processes that drive biological  
 195 systems away from thermodynamic equilibrium. Our next class of estimates consider the energy  
 196 budget of a dividing cell in terms of the synthesis of ATP from ADP and inorganic phosphate as well  
 197 as maintenance of the electrochemical proton gradient which powers it.

## 198 ATP Synthesis

199 Hydrolysis of the terminal phosphodiester bond of ATP forming ADP and an inorganic phosphate is  
 200 a kinetic driving force in a wide array of biochemical reactions. One such reaction is the formation  
 201 of peptide bonds during translation which requires  $\approx 2$  ATPs for the charging of an amino acid  
 202 to the tRNA and  $\approx 2$  ATP equivalents for the formation of the peptide bond between amino acids.  
 203 Together, these energetic costs consume  $\approx 80\%$  of the cells ATP budget (BNID: 107782; 106158;  
 204 101637; 111918, *Milo et al. (2010)*). The pool of ATP is produced by the  $F_1$ - $F_O$  ATP synthase – a  
 205 membrane-bound rotary motor which under ideal conditions can yield  $\approx 300$  ATP per second (BNID:  
 206 114701; *Milo et al. (2010); Weber and Senior (2003)*).

207 To estimate the total number of ATP equivalents consumed during a cell cycle, we will make  
 208 the approximation that there are  $\approx 3 \times 10^6$  proteins per cell with an average protein length of  $\approx$   
 209 300 peptide bonds (BNID: 115702; 108986; 104877, *Milo et al. (2010)*). Together, we arrive at the  
 210 estimate that the typical *E. coli* cell consumes  $\approx 5 \times 10^9$  ATP per cell cycle on protein synthesis  
 211 alone and  $\approx 6 \times 10^9$  ATP in total. Assuming that the ATP synthases are operating at their fastest  
 212 possible rate, we arrive at an estimate that  $\approx 3000$  ATP synthases are needed to keep up with the  
 213 energy demands of the cell. This estimate and a comparison with the data are shown in *Figure 4(A)*.  
 214 Despite our assumption of maximal ATP production rate per synthase and approximation of all NTP  
 215 consuming reactions being the same as ATP, we find that an estimate of a few thousand complete  
 216 synthases per cell to agree well with the experimental data.

## 217 Generating the Proton Electrochemical Gradient

218 In order to produce ATP, the  $F_1$ - $F_O$  ATP synthase itself must consume energy. Rather than burning  
 219 through its own product, this intricate macromolecular machine has evolved to exploit the elec-  
 220 trochemical potential established across the inner membrane through cellular respiration. This  
 221 electrochemical gradient is manifest by the pumping of protons into the intermembrane space via  
 222 the electron transport chains as they reduce NADH. In *E. coli*, this potential difference is  $\approx -200$   
 223 mV (BNID: 102120, *Milo et al. (2010)*). As estimated in the supporting information, this potential  
 224 difference is generated by maintaining  $\approx 2 \times 10^4$  protons in the intermembrane space.

225 However, the constant rotation of the ATP synthases would rapidly abolish this potential differ-  
 226 ence if it were not being actively maintained. To undergo a complete rotation (and produce a single  
 227 ATP), the  $F_1$ - $F_O$  ATP synthase must shuttle  $\approx 4$  protons across the membrane into the cytosol (BNID:  
 228 103390, *Milo et al. (2010)*). With  $\approx 3000$  ATP synthases each generating 300 ATP per second, the  
 229  $2 \times 10^4$  protons establishing the 200 mV potential would consumed in only a few milliseconds! This  
 230 brings us to our next estimate: how many electron transport complexes are needed to support  
 231 the consumption rate of the ATP synthases?

232 The electrochemistry of the electron transport complexes of *E. coli* have been the subject of  
 233 intense biochemical and biophysical study over the past half century (*Ingledew and Poole, 1984*;

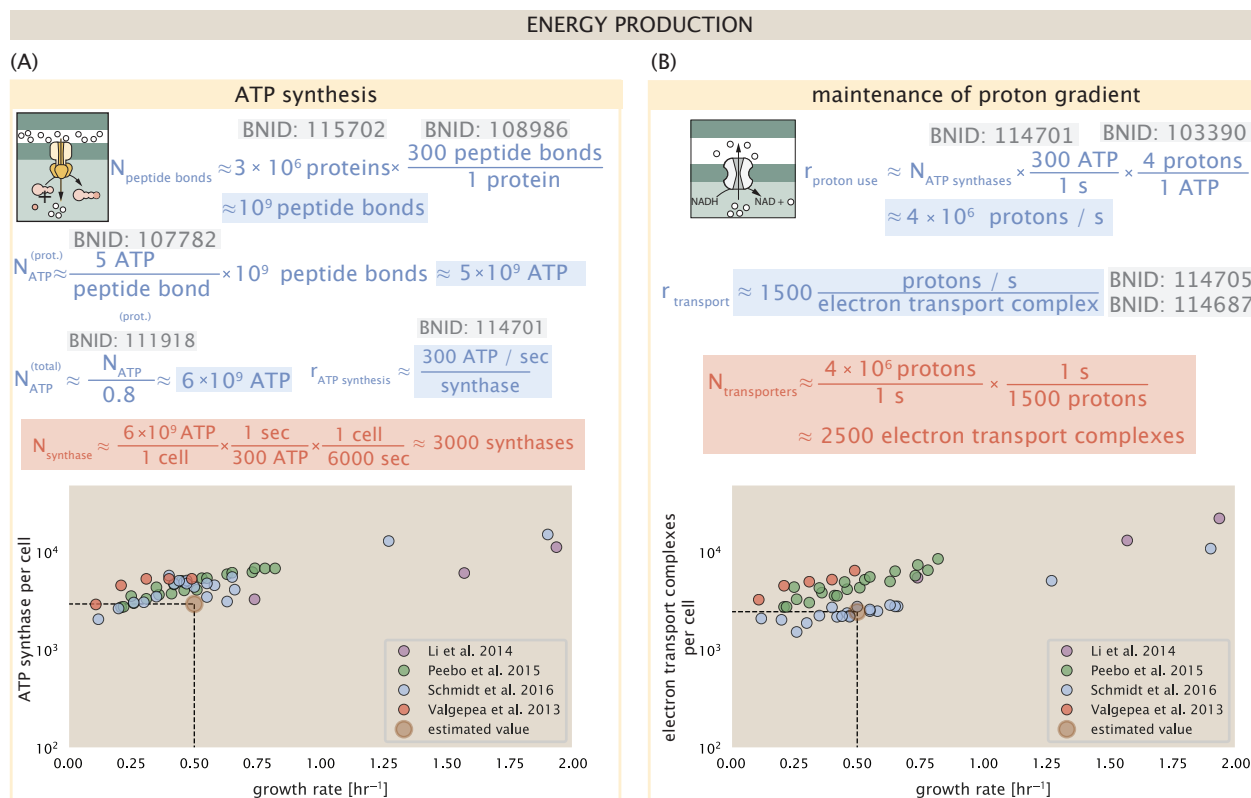


**Figure 4. The abundance of  $F_1$ - $F_O$  ATP synthases and electron transport chain complexes as a function of growth rate.** (A) Estimate of the number of  $F_1$ - $F_O$  ATP synthase complexes needed to accommodate peptide bond formation and other NTP dependent processes. Points in plot at bottom correspond to the mean number of complete  $F_1$ - $F_O$  ATP synthase complexes that can be formed given proteomic measurements and the subunit stoichiometry  $[AtpE]_{10}[AtpF]_2[AtpB][AtpC][AtpH][AtpA]_3[AtpG][AtpD]_3$ . (B) Estimate of the number of electron transport chain complexes needed to maintain a membrane potential of  $\sim -200$  mV given estimate of number of  $F_1$ - $F_O$  ATP synthases from (A). Points in plot correspond to the average number of complexes identified as being involved in aerobic respiration by the Gene Ontology identifier GO:0019646 that could be formed given proteomic observations. These complexes include cytochromes *bd1* ( $[CydA][CydB][CydX][CydH]$ ), *bdII* ( $[AppC][AppB]$ ), *bo3*, ( $[CyoD][CyoA][CyoB][CyoC]$ ) and NADH:quinone oxidoreductase I ( $[NuoA][NuoH][NuoJ][NuoK][NuoL][NuoM][NuoN][NuoB][NuoC][NuoE][NuoF][NuoG][NuoI]$ ) and II ( $[Ndh]$ ).

234     **Khademian and Imlay, 2017; Cox et al., 1970; Henkel et al., 2014.** A recent work (Szenk et al., 235 2017) examined the respiratory capacity of the *E. coli* electron transport complexes using structural 236 and biochemical data, revealing that each electron transport chain rapidly pumps protons into the 237 intermembrane space at a clip of  $\approx 5000$  protons per second (BNID: 114704; 114687, Milo et al. 238 (2010)). Using our estimate of the number of ATP synthases required per cell (Figure 4(A)), coupled 239 with these recent measurements, we estimate that  $\approx 1000$  electron transport complexes would be 240 necessary to facilitate the  $\approx 4 \times 10^6$  protons per second diet of the cellular ATP synthases. This 241 estimate is in agreement with the number of complexes identified in the proteomic datasets (plot 242 in Figure 4(B)).

#### 243     Energy production in a crowded membrane.

244     For each protein considered so far, the data shows that in general their numbers increase with 245 growth rate. This is in part a consequence of the increase in cell length and width that is common 246 to many rod-shaped bacteria at faster growth rates (Ojikic et al., 2019; Harris and Theriot, 2018). 247 For the particular case of *E. coli*, the total cellular protein and cell size increase logarithmically 248 with growth rate (Schaechter et al., 1958; Si et al., 2017). Indeed, this is one reason why we have

249 considered only a single, common growth condition across all our estimates so far. Such a scaling  
 250 will require that the total number of proteins and net demand on resources also grow in proportion  
 251 to the increase in cell size divided by the cell's doubling time. Recall however that each transport  
 252 process, as well as the ATP production via respiration, is performed at the bacterial membrane.  
 253 This means that their maximum productivity can only increase in proportion to the cell's surface  
 254 area divided by the cell doubling time. This difference in scaling would vary in proportion to the  
 255 surface area-to-volume (S/V) ratio.

256 While we found that there was more than sufficient membrane real estate for carbon intake in  
 257 our earlier estimate, the total number of ATP synthases and electron chain transport complexes  
 258 both exhibit a clear increase in copy number with growth rate, reaching in excess of  $10^4$  copies per  
 259 cell (*Figure 4*). Here we consider the consequences of this S/V ratio scaling in more detail.

260 In our estimate of ATP production above we found that a cell demands about  $6 \times 10^9$  ATP or  
 261  $10^6$  ATP/s. With a cell volume of roughly 1 fl, this corresponds to about 20 billion ATP per fl of  
 262 cell volume, in line with previous estimates (*Stouthamer and Bettenhausen, 1977; Szenk et al., 2017*). In *Figure 5A* we plot this ATP demand as a function of the S/V ratio in green, where we have  
 263 considered a range of cell shapes from spherical to rod-shaped with an aspect ratio (length/width)  
 264 equal to 4 (See appendix for calculations of cell volume and surface area). In order to consider the  
 265 maximum power that could be produced, we consider the amount of ATP that can be generated by a  
 266 membrane filled with ATP synthase and electron transport complexes, which provides a maximal  
 267 production of about 3 ATP / ( $\text{nm}^2 \cdot \text{s}$ ) (*Szenk et al., 2017*). This is shown in red in *Figure 5A*, which  
 268 shows that at least for the growth rates observed, the energy demand is roughly an order of magnitude less.  
 269 For a rod-shaped bacterium like *E. coli*, the cell volume where demand would exceed the  
 270 maximum energy production would correspond to a cell volume of about X fl. Interestingly, Szenk  
 271 et al. also found that ATP production by respiration is less efficient than by fermentation per mem-  
 272 brane area occupied due to the additional proteins of the electron transport chain. This suggests  
 273 that even under anaerobic growth, there will be sufficient membrane space for ATP production in  
 274 general.

275 While this serves to highlight the diminishing capacity to provide resources to grow if the cell  
 276 increases in size (and its S/V decreases), the blue region in *Figure 5(A)* represents a somewhat  
 277 unachievable limit since the inner membrane must also include other proteins such as those re-  
 278 quired for lipid and membrane synthesis. To gain some insight into this, we used the proteomic  
 279 data to look at the distribution of proteins on the inner membrane. Here we use Gene Ontology  
 280 (GO) annotations (*Ashburner et al., 2000; The Gene Ontology Consortium, 2018*) to identify all pro-  
 281 teins embedded or peripheral to the inner membrane (GO term: 0005886). Those associated but  
 282 not membrane-bound include proteins like MreB and ftsZ, that traverse the inner membrane by  
 283 treadmilling and must nonetheless be considered as a vital component occupying space on the  
 284 membrane. In *Figure 5(B)* we find that the total protein mass per  $\mu\text{m}$  is relatively constant with  
 285 growth rate. Interestingly, when we consider the distribution of proteins grouped by their Clusters  
 286 of Orthologous Groups (COG) (*Tatusov et al., 2000*), we find that relative abundance for those in  
 287 metabolism (including ATP synthesis via respiration) is also relatively constant.

## 289 Synthesis of the Cell Wall and lipid membrane.

290 [To be completed.]

## 291 Function of the Central Dogma

292 Up to this point, we have considered a variety of transport and biosynthetic processes that are  
 293 critical to acquiring and generating new cell mass. While there are of course many other metabolic  
 294 processes we could consider and perform estimates of (such as the components of fermentative  
 295 versus aerobic respiration), we now turn our focus to some of the most central processes which  
 296 must be undertaken irrespective of the growth conditions – the processes of the central dogma.

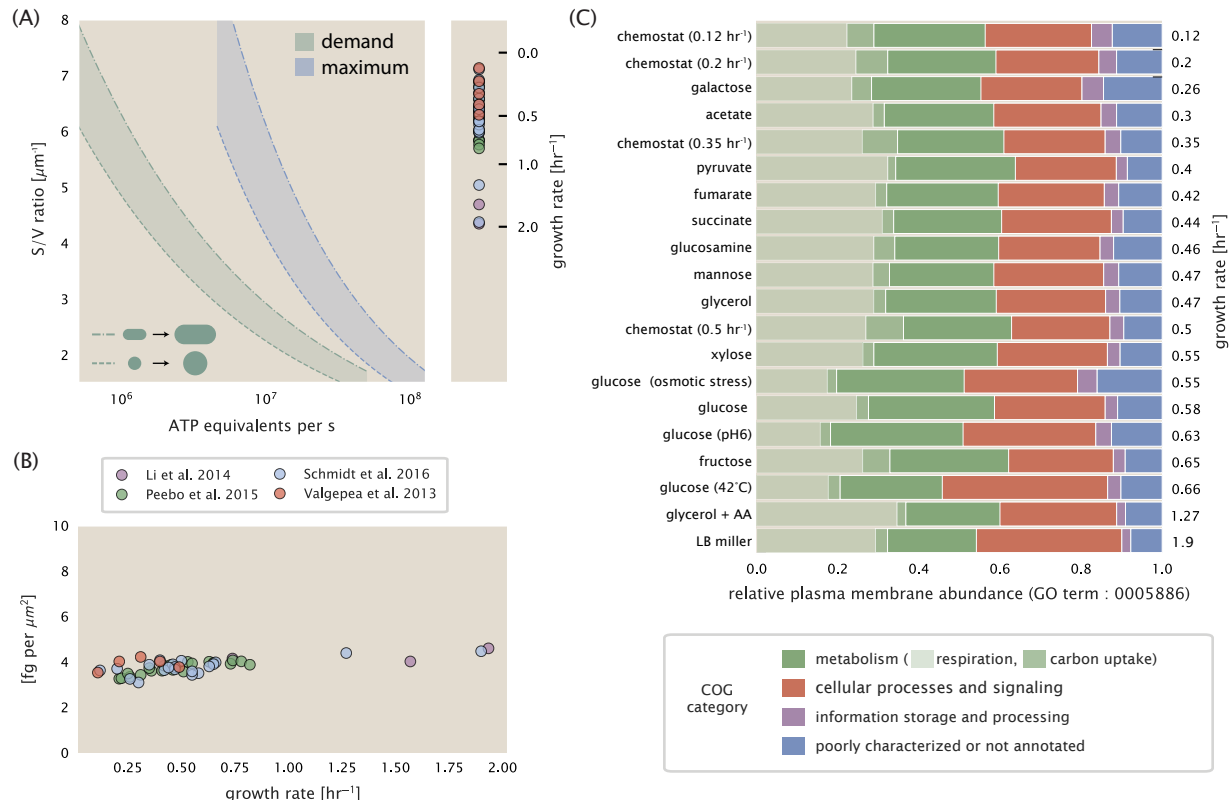


**Figure 5. Influence of cell size and S/V ratio on ATP production and inner membrane composition.** (A) Scaling of ATP demand and maximum ATP production as a function of S/V ratio. Cell volumes of 0.5 fl to 50 fl were considered, with the dash line corresponding to a cell with spherical shape, which the dash-dot line reflects a rod-shaped bacterium like *E. coli* with aspect ratio of 4. 50% of the bacterial inner membrane is assumed to be protein, with the remainder lipid. (B) Total protein mass calculated for proteins with inner membrane annotation (GO term: 0005886). (C) Relative protein abundances by mass based on COG annotation. Metabolic proteins are further separated into respiration ( $F_1$ - $F_O$  ATP synthase, NADH dehydrogenase I, succinate:quinone oxidoreductase, cytochrome  $b_0$  $_3$  ubiquinol oxidase, cytochrome bd-I ubiquinol oxidase) and carbohydrate transport (GO term: GO:0008643). Note that the elongation factor EF-Tu can also associate with the inner membrane, but was excluded in this analysis due to its high relative abundance (roughly identical to the total mass shown in part (B)).

**297 DNA**

298 Most bacteria (including *E. coli*) harbor a single, circular chromosome and can have extra-chromosomal  
 299 plasmids ~ 100 kbp in length. We will focus our quantitative thinking solely on the chromosome  
 300 of *E. coli* which harbors ≈ 5000 genes and ≈ 5 × 10<sup>6</sup> base pairs. To successfully divide and produce  
 301 viable progeny, this chromosome must be faithfully replicated and segregated into each nascent  
 302 cell. We again rely on the near century of literature in molecular biology to provide some insight  
 303 towards the rates and mechanics of the replicative feat as well as the production of the replication  
 304 starting materials, dNTPs.

**305 dNTP synthesis**

306 We begin our exploration of the DNA replicative processes by examining the production of the de-  
 307 oxyribonucleotide triphosphates (dNTPs). The four major dNTPS (dATP, dTTP, dCTP, and dGTP) are  
 308 synthesized *de novo* in separate pathways, requiring different building blocks. However, a critical  
 309 step present in all dNTP synthesis pathways is the conversion from ribonucleotide to deoxyribonu-  
 310 cleotide via the removal of the 3' hydroxyl group of the ribose ring CITE. This reaction is mediated  
 311 by a class of enzymes termed ribonucleotide reductases, of which *E. coli* possesses two aerobically  
 312 active complexes (termed I and II) and a single anaerobically active enzyme CITE. Due to their pecu-  
 313 liar formation of a peculiar radical intermediate, these enzymes have received much biochemical  
 314 kinetic and structural characterization. One such work (*Ge et al., 2003*) performed a detailed *in*  
 315 *vitro* measurement of the steady-state kinetic rates of these complexes, revealing a turnover rate  
 316 of ≈ 10 per second.

317 Considering this reaction (mediated by the ribonucleotide reductase complexes I and II) is cen-  
 318 tral to synthesis of all dNTPS, it is reasonable to consider the abundance of these complexes as a  
 319 measure of the total dNTP production in *E. coli*. Illustrated schematically in ??(A), we consider the  
 320 fact that to replicate the cell's genome, on the order of ≈ 10<sup>7</sup> dNTPs must be synthesized. Assum-  
 321 ing a production rate of 10 per second per ribonucleotide reductase complex and a cell division  
 322 time of 6000 seconds, we arrive at an estimate of ≈ 150 complexes are needed per cell. As shown  
 323 in the bottom panel of ??(A), this estimate agrees with the experimental measurements of these  
 324 complexes abundances within ≈ 1/2 an order of magnitude.

325 Recent work has that during replication, the ribonucleotide reductases complexes localize into  
 326 discrete foci colocalized with the DNA replisome complex (*Sánchez-Romero et al., 2011*). This is  
 327 particularly pronounced in environments where growth is slow, indicating that spatial organization  
 328 and regulation of the activity of the complexes plays an important role.

**329 DNA Replication**

330 We now turn our focus towards the process of integration of the dNTP building blocks into the  
 331 replicated chromosome strand via the DNA polymerase enzymes. Replication of bacterial chro-  
 332 mosomes is initiated at a single region of the chromosome termed the *oriC* locus at which a pair  
 333 of DNA polymerases bind and begin their high-fidelity replication of the genome in opposite di-  
 334 rections. Assuming equivalence between the two replication forks, this means that the two DNA  
 335 polymerases meet at the midway point of the circular chromosome termed the *ter* locus. This divi-  
 336 sion of labor means The kinetics of the four types of DNA polymerases (I – V) have been intensely  
 337 studied, revealing that DNA polymerase III performs the high fidelity processive replication of the  
 338 genome with the other "accessory" polymerases playing auxiliary roles *Fijalkowska et al. (2012)*. *In*  
 339 *vitro* measurements have shown that DNA Polymerase III copies DNA at a rate of ≈ 600 nucleotides  
 340 per second (BNID: 104120, *Milo et al. (2010)*). Thus, to replicate a single chromosome, two DNA  
 341 polymerases replicating at their maximal rate would copy the entire genome in ≈ 4000 s. Thus,  
 342 with a division time of 6000 s (our "typical" growth rate for the purposes of this work), there is suf-  
 343 ficient time for a pair of DNA polymerases to replicate the entire genome. However, this estimate  
 344 implies that 4000 s would be the upper-limit time scale for bacterial division which is at odds with  
 345 the familiar ≈ 1500 s doubling time of *E. coli* in rich medium.

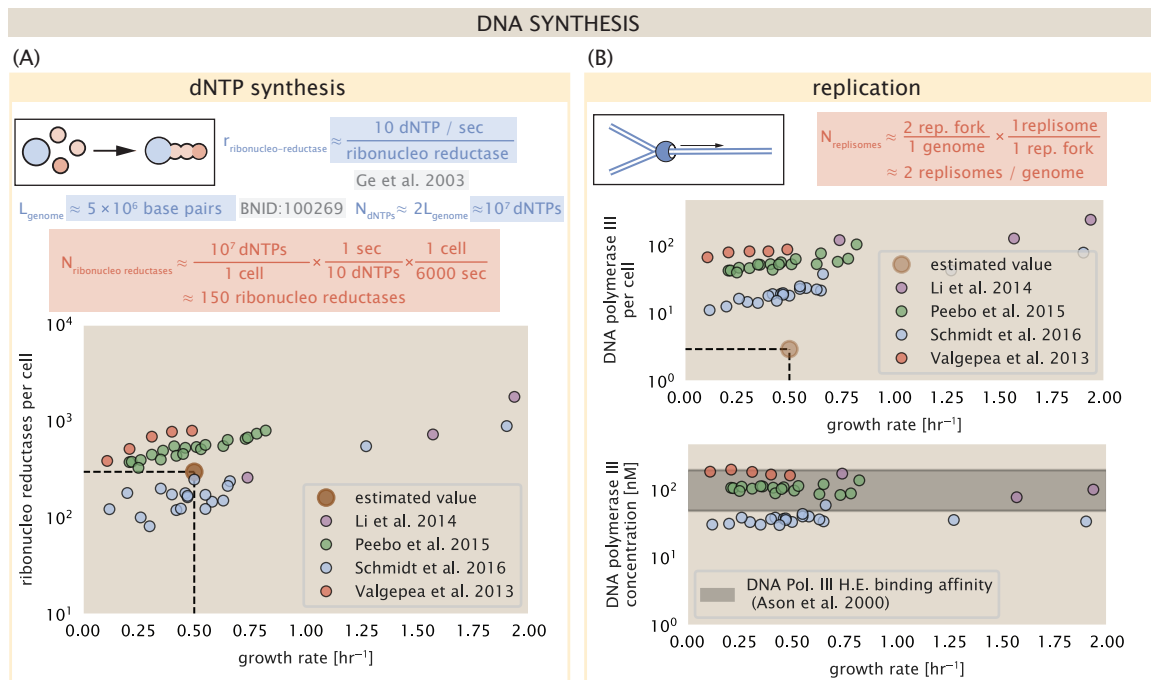


**Figure 6. Complex abundance estimates for dNTP synthesis and DNA replication.** (A) Estimate of the number of ribonucleotide reductases enzymes needed to facilitate the synthesis of  $\approx 10^7$  dNTPs over the course of a 6000 second generation time. Points in the plot correspond to the total number of ribonucleotide reductase I ( $[NrdA]_2[NrdB]_2$ ) and ribonucleotide reductase II ( $[NrdE]_2[NrdF]_2$ ) complexes. (B) An estimate for the minimum number of DNA polymerases holoenzyme complexes needed to facilitate replication of a single genome. Points in the top plot correspond to the total number of DNA polymerase III holoenzyme complexes ( $[DnaE]_3[DnaQ]_3[HolE]_3[DnaX]_5[HolB][HolA][DnaN]_4[HolC]_4[HolD]_4$ ) per cell. Bottom plot shows the effective concentration of DNA polymerase III holoenzyme given cell volumes calculated from the growth rate as in *Si et al. (2019)*.

346 It is known well known that *E. coli* can parallelize its DNA replication such that multiple chromo-  
 347 somes are being replicated at once. Recent work (*Si et al., 2017*) has shown that the replicative  
 348 timescale of cell division can be massively parallelized where *E. coli* can have on the order of 10 -  
 349 12 replication forks at a given time. Thus, even in rapidly growing cultures, only a few polymerases  
 350 ( $\approx 10$ ) are needed to replicate the chromosome. However, as shown in ??(B), DNA polymerase III is  
 351 nearly an order of magnitude more abundant. This discrepancy can be understood when  
 352 considering the binding affinities. The DNA polymerase III complex is highly processive, facilitated  
 353 by a strong affinity of the complex to the DNA. *In vitro* biochemical characterization has quantified  
 354 the  $K_D$  of DNA polymerase III holoenzyme to single-stranded and double-stranded DNA to be 50  
 355 and 200 nM, respectively. The bottom plot in *Figure 6(B)* shows that the concentration of the DNA  
 356 polymerase III across all data sets and growth conditions is within this range (*Ason et al., 2000*).  
 357 Thus, while the copy number of the DNA polymerase III is in excess of the strict number required  
 358 to replicate the genome, the copy number is tuned such that the concentration is approximately  
 359 equal to the dissociation constant to the DNA. While the processes regulating the initiation of DNA  
 360 replication are complex and involve more than just the holoenzyme, these data indicate that the  
 361 kinetics of replication rather than the explicit copy number of the DNA polymerase III holoenzyme  
 362 is the more relevant feature of DNA replication to consider.

### 363 Protein synthesis

364 Lastly, we turn our attention to the process of translation. So far in our various estimates there  
 365 has been little to suggest any apparent limit to how fast a bacterium might divide under steady-  
 366 state growth. Even in our examples of *E. coli* grown rapidly under different carbohydrate sources  
 367 (*Figure 2(B)*), cells are able to utilize less preferred carbon sources by inducing the expression of  
 368 additional membrane transporters and enzymes. [Maybe go into Hwa style resource allocation  
 369 with references added]. In this respect, gross overexpression of a protein can lead to a reduction  
 370 of the growth rate.

371 We can determine the translation-limited growth rate by noting that the total number of peptide  
 372 bonds created as the cell doubles  $N_{aa}$  will be given by,  $\tau \cdot r_t \cdot R$ . Here,  $\tau$  refers to the doubling time of  
 373 the cell under steady-state growth,  $r_t$  is the maximum translation rate, and  $R$  is the average number  
 374 of ribosomes in the cell. With the growth rate related to the cell doubling time by  $\lambda = \ln(2)/\tau$ , we  
 375 can write the translation-limited growth rate as,

$$\lambda_{\text{translation-limited}} = \frac{\ln(2) \cdot r_t \cdot R}{N_{aa}}. \quad (1)$$

376 Alternatively, since  $N_{aa}$  is related to the total protein mass through the molecular weight of each  
 377 protein, we can also consider the growth rate in terms of ribosomal mass fraction. This calculation  
 378 is shown in *Figure 7(A)*. This allows us to rewrite the growth rate as,

$$\lambda_{\text{translation-limited}} \approx \frac{\ln(2) \cdot r_t}{L_R} \Phi_R, \quad (2)$$

379 where  $L_R$  is the total length in amino acids that make up a ribosome, and  $\Phi_R$  is the ribosomal mass  
 380 fraction. This is plotted as a function of ribosomal fraction  $\Phi_R$  in *Figure 7(A)*, with a translation rate  
 381  $r_t = 17 \text{ aa/s}$  and  $L_R = 10^6 \text{ aa}$ , which corresponds to the length in amino acids for all ribosomal subunits  
 382 of the 50S and 30S complexes and elongation factor required for translation.

383 Perhaps the first thing to notice is that there is a maximum growth rate at about  $\lambda \approx 6 \text{ hr}^{-1}$ , or  
 384 doubling time of about 7 minutes. This maximum growth rate can be viewed as an inherent speed  
 385 limit due to the need for the cell to double the cell's entire ribosomal mass. Interestingly, this limit is  
 386 independent of the absolute number of ribosomes, but rather is simply given by time to translate  
 387 an entire ribosome,  $L_R/r_t$ . As shown in *Figure 7(B)*, we can reconcile this with the observation  
 388 that in order to double the average number of ribosomes, each ribosome must produce a second  
 389 ribosome. This is a process that cannot be parallelized further.

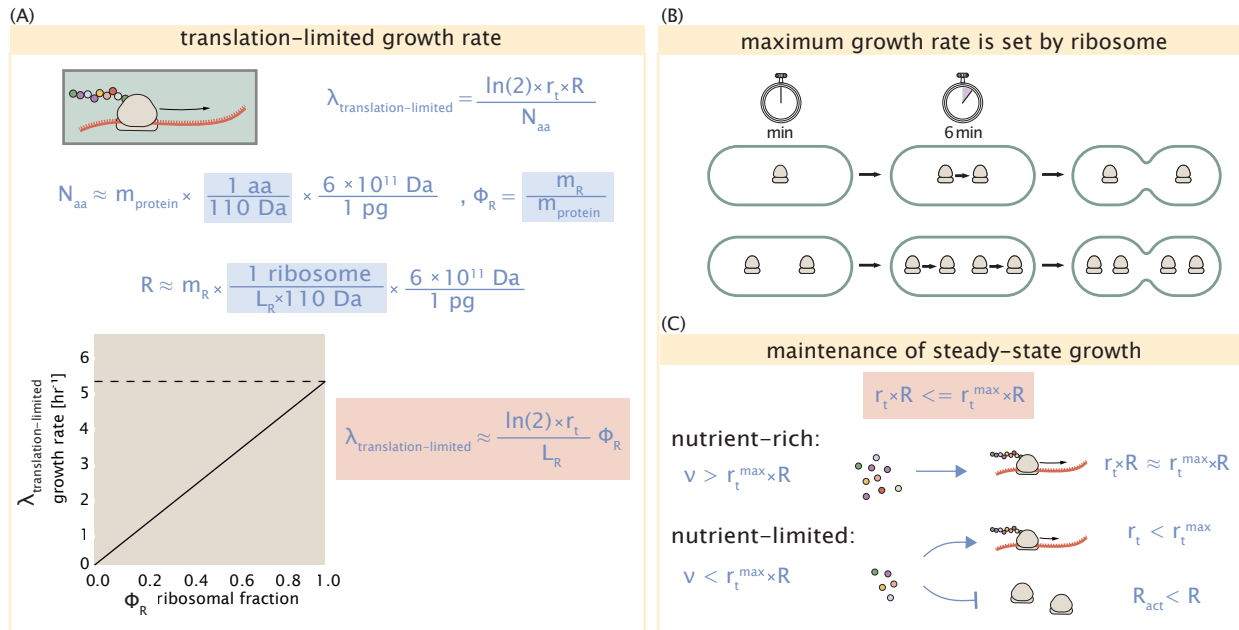


**Figure 7. Translation-limited growth rate.** (A) Here we consider the translation-limited growth rate as a function of ribosomal fraction. By mass balance, the time required to double the entire proteome ( $N_{\text{aa}} / r_t$ ) sets the translation-limited growth rate,  $\lambda_{\text{translation-limited}}$ . Here  $N_{\text{aa}}$  is effectively the number of peptide bonds that must be translated,  $r_t$  is the translation elongation rate, and  $R$  is the number of ribosomes. This can also be re-written in terms of the ribosomal mass fraction  $\Phi_R = m_R / m_{\text{protein}}$ , where  $m_R$  is the total ribosomal mass and  $m_{\text{protein}}$  is the mass of all proteins in the cell.  $L_R$  refers to the summed length of the ribosome in amino acids.  $\lambda_{\text{translation-limited}}$  is plotted as a function of  $\Phi_R$  (solid line). (B) The dashed line in part (A) identifies a maximum growth rate that is set by the ribosome. Specifically, this growth rate corresponds to the time required to translate an entire ribosome,  $L_R / r_t$ . This is a result that is independent of the number of ribosomes in the cell as shown schematically here. (C)

390 Since a cell consists of more than just ribosomes, we can see that for  $\Phi_R$  in the range of about  
 391 0.1 - 0.3, the maximum growth rate is in line with experimentally reported growth rates around  
 392 0.5 - 2  $\text{hr}^{-1}$ . Here we have implicitly assumed that translation proceeds randomly, without pref-  
 393 erence between ribosomal or non-ribosomal mRNA, which appears reasonable. Importantly, in  
 394 order for a cell to scale this limit set by  $\Phi_R$  the cell must increase its ribosomal abundance, either  
 395 by synthesizing more ribosomes or reducing the fraction of non-ribosomal proteins.

396 One additional point to note is that across different species of bacteria, cells do not decrease  
 397 their ribosomal abundance to zero in the limit of poorer nutrient condition [CITE?]. Indeed, some  
 398 organisms appear to have constant ribosomal abundance irrespective of their growth rate [NB:  
 399 ask Griffin and figure out what organism this is]. From the perspective of a bacterium dealing with  
 400 uncertain nutrient conditions, there is likely a benefit for the cell to maintain some relative frac-  
 401 tion of ribosomes to support rapid growth as nutrient conditions improve. In addition, given their  
 402 massive size at about 850 kDa, they may play an as-yet fully understood role as a crowding agent  
 403 in cellular function *Delarue et al. (2018); Soler-Bistué et al. (2020)*. If we consider a scenario where  
 404 nutrient conditions become poorer and poorer, there must be a regime where the cell has more  
 405 ribosomes than it can utilize. While this perhaps suggests less import to the process of translation,  
 406 it is important to recognize that in order for a cell to maintain steady-state growth, the cell's transla-  
 407 tion capacity must be mitigated. Otherwise, ribosomes will deplete their supply of amino acids and  
 408 this will bring translation and cell growth to a halt (*Figure 7(C)*). We will consider the consequences  
 409 of this in the case of *E. coli* next.

**Figure 8.** . (A) (B) (C).**410    Multiple replication forks provide one strategy to support faster growth.**

411    We now turn to our proteomic data from *E. coli* and plot the ribosomal fraction as a function of  
 412    reported growth rate. Here we find that the ribosomal fraction always increases with growth rate.  
 413    This is consistent with the behavior expected for *E. coli*, and an observation of intense study related  
 414    to the so-called nutrient-limited growth law. In terms of absolute ribosomal abundance, we find  
 415    that cells increase both their quantity and cellular concentration at faster growth.

416       One feature of *E. coli*, as well as other bacteria like *B. subtilis*, is the ability to begin replication of  
 417    multiple copies of its genome during a single cell cycle. This is achieved through multiple initiation  
 418    forks and nested DNA replication. [need to refer to work from Jun lab here!! - under adder  
 419    mechanism, the cell appears to add a certain cell mass in proportion to its number of origins]. We  
 420    find that the ribosome copy number increases in proportion to the expected number of origins.  
 421    The process of nested DNA replication will lead to a bias in gene dosage for genes closer to the  
 422    origin of replication () Importantly, ribosomal protein and rRNA genes are closer to the origin of  
 423    replication *Scholz et al. (2019)* and this provides a natural way for *E. coli* to bias the proportion  
 424    of ribosomes at faster growth without the advent of additional gene regulation strategies. Given  
 425    that ribosomal genes in *E. coli* appear to be transcribed at their maximal rate at fast growth rates  
 426    [cite??], increasing ribosomal copy number through increased gene dosage represents a creative  
 427    approach for the cell to grow faster without gross down-regulation of non-ribosomal genes.

**428    References**

- 429    Aidelberg, G., Towbin, B. D., Rothschild, D., Dekel, E., Bren, A., and Alon, U. (2014). Hierarchy of non-glucose  
 430    sugars in *Escherichia coli*. *BMC Systems Biology*, 8(1):133.
- 431    Antonenko, Y. N., Pohl, P., and Denisov, G. A. (1997). Permeation of ammonia across bilayer lipid membranes  
 432    studied by ammonium ion selective microelectrodes. *Biophysical Journal*, 72(5):2187–2195.
- 433    Ashburner, M., Ball, C. A., Blake, J. A., Botstein, D., Butler, H., Cherry, J. M., Davis, A. P., Dolinski, K., Dwight, S. S.,  
 434    Eppig, J. T., Harris, M. A., Hill, D. P., Issel-Tarver, L., Kasarskis, A., Lewis, S., Matese, J. C., Richardson, J. E.,  
 435    Ringwald, M., Rubin, G. M., and Sherlock, G. (2000). Gene Ontology: tool for the unification of biology. *Nature  
 436    Genetics*, 25(1):25–29.
- 437    Ason, B., Bertram, J. G., Hingorani, M. M., Beechem, J. M., O'Donnell, M., Goodman, M. F., and Bloom, L. B.  
 438    (2000). A Model for *Escherichia coli* DNA Polymerase III Holoenzyme Assembly at Primer/Template Ends:  
 439    DNA Triggers A Change In Binding Specificity of the  $\gamma$  Complex Clamp Loader. *Journal of Biological Chemistry*,  
 440    275(4):3006–3015.
- 441    Assentoft, M., Kaptan, S., Schneider, H.-P., Deitmer, J. W., de Groot, B. L., and MacAulay, N. (2016). Aquaporin 4  
 442    as a NH<sub>3</sub> Channel. *Journal of Biological Chemistry*, 291(36):19184–19195.
- 443    Basan, M., Zhu, M., Dai, X., Warren, M., Sévin, D., Wang, Y.-P., and Hwa, T. (2015). Inflating bacterial cells by  
 444    increased protein synthesis. *Molecular Systems Biology*, 11(10):836.
- 445    Bauer, S. and Ziv, E. (1976). Dense growth of aerobic bacteria in a bench-scale fermentor. *Biotechnology and  
 446    Bioengineering*, 18(1):81–94. \_eprint: <https://onlinelibrary.wiley.com/doi/10.1002/bit.260180107>.
- 447    Belliveau, N. M., Barnes, S. L., Ireland, W. T., Jones, D. L., Sweredoski, M. J., Moradian, A., Hess, S., Kinney, J. B.,  
 448    and Phillips, R. (2018). Systematic approach for dissecting the molecular mechanisms of transcriptional  
 449    regulation in bacteria. *Proceedings of the National Academy of Sciences*, 115(21):E4796–E4805.
- 450    Booth, I. R., Mitchell, W. J., and Hamilton, W. A. (1979). Quantitative analysis of proton-linked transport systems.  
 451    The lactose permease of *Escherichia coli*. *Biochemical Journal*, 182(3):687–696.
- 452    Cox, G. B., Newton, N. A., Gibson, F., Snoswell, A. M., and Hamilton, J. A. (1970). The function of ubiquinone in  
 453    *Escherichia coli*. *Biochemical Journal*, 117(3):551–562.

- 454 Delarue, M., Brittingham, G. P., Pfeffer, S., Surovtsev, I. V., Pinglay, S., Kennedy, K. J., Schaffer, M., Gutierrez,  
 455 J. I., Sang, D., Poterewicz, G., Chung, J. K., Plitzko, J. M., Groves, J. T., Jacobs-Wagner, C., Engel, B. D., and Holt,  
 456 L. J. (2018). mTORC1 Controls Phase Separation and the Biophysical Properties of the Cytoplasm by Tuning  
 457 Crowding. *Cell*, 174(2):338–349.e20.
- 458 Escalante, A., Salinas Cervantes, A., Gosset, G., and Bolívar, F. (2012). Current knowledge of the Escherichia coli  
 459 phosphoenolpyruvate–carbohydrate phosphotransferase system: Peculiarities of regulation and impact on  
 460 growth and product formation. *Applied Microbiology and Biotechnology*, 94(6):1483–1494.
- 461 Feist, A. M., Henry, C. S., Reed, J. L., Krummenacker, M., Joyce, A. R., Karp, P. D., Broadbelt, L. J., Hatzimanikatis,  
 462 V., and Palsson, B. Ø. (2007). A genome-scale metabolic reconstruction for Escherichia coli K-12 MG1655 that  
 463 accounts for 1260 ORFs and thermodynamic information. *Molecular Systems Biology*, 3(1):121.
- 464 Fijalkowska, I. J., Schaaper, R. M., and Jonczyk, P. (2012). DNA replication fidelity in Escherichia coli: A multi-DNA  
 465 polymerase affair. *FEMS Microbiology Reviews*, 36(6):1105–1121.
- 466 Gama-Castro, S., Salgado, H., Santos-Zavaleta, A., Ledezma-Tejeida, D., Muñiz-Rascado, L., García-Sotelo, J. S.,  
 467 Alquicira-Hernández, K., Martínez-Flores, I., Pannier, L., Castro-Mondragón, J. A., Medina-Rivera, A., Solano-  
 468 Lira, H., Bonavides-Martínez, C., Pérez-Rueda, E., Alquicira-Hernández, S., Porrón-Sotelo, L., López-Fuentes,  
 469 A., Hernández-Koutoucheva, A., Moral-Chávez, V. D., Rinaldi, F., and Collado-Vides, J. (2016). RegulonDB  
 470 version 9.0: High-level integration of gene regulation, coexpression, motif clustering and beyond. *Nucleic  
 471 Acids Research*, 44(D1):D133–D143.
- 472 Ge, J., Yu, G., Ator, M. A., and Stubbe, J. (2003). Pre-Steady-State and Steady-State Kinetic Analysis of *E. coli* Class  
 473 I Ribonucleotide Reductase. *Biochemistry*, 42(34):10071–10083.
- 474 Harris, L. K. and Theriot, J. A. (2018). Surface Area to Volume Ratio: A Natural Variable for Bacterial Morphogenesis.  
 475 *Trends in microbiology*, 26(10):815–832.
- 476 Harris, R. M., Webb, D. C., Howitt, S. M., and Cox, G. B. (2001). Characterization of PitA and PitB from *Escherichia  
 477 coli*. *Journal of Bacteriology*, 183(17):5008–5014.
- 478 Heldal, M., Norland, S., and Tumyr, O. (1985). X-ray microanalytic method for measurement of dry matter and  
 479 elemental content of individual bacteria. *Applied and Environmental Microbiology*, 50(5):1251–1257.
- 480 Henkel, S. G., Beek, A. T., Steinsiek, S., Stagge, S., Bettenbrock, K., de Mattos, M. J. T., Sauter, T., Sawodny, O.,  
 481 and Ederer, M. (2014). Basic Regulatory Principles of Escherichia coli's Electron Transport Chain for Varying  
 482 Oxygen Conditions. *PLoS ONE*, 9(9):e107640.
- 483 Hui, S., Silverman, J. M., Chen, S. S., Erickson, D. W., Basan, M., Wang, J., Hwa, T., and Williamson, J. R. (2015).  
 484 Quantitative proteomic analysis reveals a simple strategy of global resource allocation in bacteria. *Molecular  
 485 Systems Biology*, 11(2):e784–e784.
- 486 Ingledew, W. J. and Poole, R. K. (1984). The respiratory chains of Escherichia coli. *Microbiological Reviews*,  
 487 48(3):222–271.
- 488 Ireland, W. T., Beeler, S. M., Flores-Bautista, E., Belliveau, N. M., Sweredoski, M. J., Moradian, A., Kinney, J. B.,  
 489 and Phillips, R. (2020). Deciphering the regulatory genome of *Escherichia coli*, one hundred promoters at a  
 490 time. *bioRxiv*.
- 491 Jacob, F. and Monod, J. (1961). Genetic regulatory mechanisms in the synthesis of proteins. *Journal of Molecular  
 492 Biology*, 3(3):318–356.
- 493 Jun, S., Si, F., Pugatch, R., and Scott, M. (2018). Fundamental principles in bacterial physiology - history, recent  
 494 progress, and the future with focus on cell size control: A review. *Reports on Progress in Physics*, 81(5):056601.
- 495 Khademi, S., O'Connell, J., Remis, J., Robles-Colmenares, Y., Miercke, L.J.W., and Stroud, R. M. (2004). Mechanism  
 496 of Ammonia Transport by Amt/MEP/Rh: Structure of AmtB at 1.35 Å. *Science*, 305(5690):1587–1594.
- 497 Khademian, M. and Imlay, J. A. (2017). *Escherichia Coli* cytochrome c peroxidase is a respiratory oxidase that  
 498 enables the use of hydrogen peroxide as a terminal electron acceptor. *Proceedings of the National Academy  
 499 of Sciences*, 114(33):E6922–E6931.
- 500 Li, G.-W., Burkhardt, D., Gross, C., and Weissman, J. S. (2014). Quantifying absolute protein synthesis rates  
 501 reveals principles underlying allocation of cellular resources. *Cell*, 157(3):624–635.

- 502 Liu, M., Durfee, T., Cabrera, J. E., Zhao, K., Jin, D. J., and Blattner, F. R. (2005). Global Transcriptional Programs  
 503 Reveal a Carbon Source Foraging Strategy by *Escherichia coli*. *Journal of Biological Chemistry*, 280(16):15921–  
 504 15927.
- 505 Milo, R., Jorgensen, P., Moran, U., Weber, G., and Springer, M. (2010). BioNumbers—the database of key num-  
 506 bers in molecular and cell biology. *Nucleic Acids Research*, 38(suppl\_1):D750–D753.
- 507 Monod, J. (1947). The phenomenon of enzymatic adaptation and its bearings on problems of genetics and  
 508 cellular differentiation. *Growth Symposium*, 9:223–289.
- 509 Neidhardt, F. C., Ingraham, J., and Schaechter, M. (1991). *Physiology of the Bacterial Cell - A Molecular Approach*,  
 510 volume 1. Elsevier.
- 511 Ojkic, N., Serbanescu, D., and Banerjee, S. (2019). Surface-to-volume scaling and aspect ratio preservation in  
 512 rod-shaped bacteria. *eLife*, 8:642.
- 513 Peebo, K., Valgepea, K., Maser, A., Nahku, R., Adamberg, K., and Vilu, R. (2015). Proteome reallocation in *Es-  
 514 cherichia coli* with increasing specific growth rate. *Molecular BioSystems*, 11(4):1184–1193.
- 515 Phillips, R. (2018). Membranes by the Numbers. In *Physics of Biological Membranes*, pages 73–105. Springer,  
 516 Cham, Cham.
- 517 Ramos, S. and Kaback, H. R. (1977). The relation between the electrochemical proton gradient and active trans-  
 518 port in *Escherichia coli* membrane vesicles. *Biochemistry*, 16(5):854–859.
- 519 Rosenberg, H., Gerdes, R. G., and Chegwidden, K. (1977). Two systems for the uptake of phosphate in *Es-  
 520 cherichia coli*. *Journal of Bacteriology*, 131(2):505–511.
- 521 Sánchez-Romero, M. A., Molina, F., and Jiménez-Sánchez, A. (2011). Organization of ribonucleoside diphosphate  
 522 reductase during multifork chromosome replication in *Escherichia coli*. *Microbiology*, 157(8):2220–2225.
- 523 Schaechter, M., Maaløe, O., and Kjeldgaard, N. O. (1958). Dependency on Medium and Temperature of Cell Size  
 524 and Chemical Composition during Balanced Growth of *Salmonella typhimurium*. *Microbiology*, 19(3):592–606.
- 525 Schmidt, A., Kochanowski, K., Vedelaar, S., Ahrné, E., Volkmer, B., Callipo, L., Knoops, K., Bauer, M., Aebersold,  
 526 R., and Heinemann, M. (2016). The quantitative and condition-dependent *Escherichia coli* proteome. *Nature  
 527 Biotechnology*, 34(1):104–110.
- 528 Scholz, S. A., Diao, R., Wolfe, M. B., Fivenson, E. M., Lin, X. N., and Freddolino, P. L. (2019). High-Resolution  
 529 Mapping of the *Escherichia coli* Chromosome Reveals Positions of High and Low Transcription. *Cell Systems*,  
 530 8(3):212–225.e9.
- 531 Scott, M., Gunderson, C. W., Mateescu, E. M., Zhang, Z., and Hwa, T. (2010). Interdependence of cell growth and  
 532 gene expression: origins and consequences. *Science*, 330(6007):1099–1102.
- 533 Sekowska, A., Kung, H.-F., and Danchin, A. (2000). Sulfur Metabolism in *Escherichia coli* and Related Bacteria:  
 534 Facts and Fiction. *Journal of Molecular Microbiology and Biotechnology*, 2(2):34.
- 535 Si, F., Le Treut, G., Sauls, J. T., Vadia, S., Levin, P. A., and Jun, S. (2019). Mechanistic Origin of Cell-Size Control  
 536 and Homeostasis in Bacteria. *Current Biology*, 29(11):1760–1770.e7.
- 537 Si, F., Li, D., Cox, S. E., Sauls, J. T., Azizi, O., Sou, C., Schwartz, A. B., Erickstad, M. J., Jun, Y., Li, X., and Jun, S. (2017).  
 538 Invariance of Initiation Mass and Predictability of Cell Size in *Escherichia coli*. *Current Biology*, 27(9):1278–  
 539 1287.
- 540 Sirko, A., Zatyka, M., Sadowy, E., and Hulanicka, D. (1995). Sulfate and thiosulfate transport in *Escherichia coli* K-  
 541 12: Evidence for a functional overlapping of sulfate- and thiosulfate-binding proteins. *Journal of Bacteriology*,  
 542 177(14):4134–4136.
- 543 Soler-Bistué, A., Aguilar-Pierlé, S., Garcia-Garcerá, M., Val, M.-E., Sismeiro, O., Varet, H., Sieira, R., Krin, E., Skov-  
 544 gaard, O., Comerci, D. J., Eduardo P. C. Rocha, and Mazel, D. (2020). Macromolecular crowding links ribosomal  
 545 protein gene dosage to growth rate in *Vibrio cholerae*. *BMC Biology*, 18(1):1–18.
- 546 Stasi, R., Neves, H. I., and Spira, B. (2019). Phosphate uptake by the phosphonate transport system PhnCDE.  
 547 *BMC Microbiology*, 19.
- 548 Stouthamer, A. H. and Bettenhaussen, C. W. (1977). A continuous culture study of an ATPase-negative mutant  
 549 of *Escherichia coli*. *Archives of Microbiology*, 113(3):185–189.

- 550 Szenk, M., Dill, K. A., and de Graff, A. M. R. (2017). Why Do Fast-Growing Bacteria Enter Overflow Metabolism?  
551 Testing the Membrane Real Estate Hypothesis. *Cell Systems*, 5(2):95–104.
- 552 Tatusov, R. L., Galperin, M. Y., Natale, D. A., and Koonin, E. V. (2000). The COG database: a tool for genome-scale  
553 analysis of protein functions and evolution. *Nucleic Acids Research*, 28(1):33–36.
- 554 Taymaz-Nikerel, H., Borujeni, A. E., Verheijen, P. J. T., Heijnen, J. J., and van Gulik, W. M. (2010).  
555 Genome-derived minimal metabolic models for *Escherichia coli* MG1655 with estimated in  
556 vivo respiratory ATP stoichiometry. *Biotechnology and Bioengineering*, 107(2):369–381. \_eprint:  
557 <https://onlinelibrary.wiley.com/doi/pdf/10.1002/bit.22802>.
- 558 The Gene Ontology Consortium (2018). The Gene Ontology Resource: 20 years and still GOing strong. *Nucleic  
559 Acids Research*, 47(D1):D330–D338.
- 560 Valgepea, K., Adamberg, K., Seiman, A., and Vilu, R. (2013). *Escherichia coli* achieves faster growth by increasing  
561 catalytic and translation rates of proteins. *Molecular BioSystems*, 9(9):2344.
- 562 van Heeswijk, W. C., Westerhoff, H. V., and Boogerd, F. C. (2013). Nitrogen Assimilation in *Escherichia coli*: Putting  
563 Molecular Data into a Systems Perspective. *Microbiology and Molecular Biology Reviews*, 77(4):628–695.
- 564 Weber, J. and Senior, A. E. (2003). ATP synthesis driven by proton transport in F1F0-ATP synthase. *FEBS Letters*,  
565 545(1):61–70.
- 566 Willsky, G. R., Bennett, R. L., and Malamy, M. H. (1973). Inorganic Phosphate Transport in *Escherichia coli*:  
567 Involvement of Two Genes Which Play a Role in Alkaline Phosphatase Regulation. *Journal of Bacteriology*,  
568 113(2):529–539.
- 569 Zhang, L., Jiang, W., Nan, J., Almqvist, J., and Huang, Y. (2014a). The *Escherichia coli* CysZ is a pH dependent  
570 sulfate transporter that can be inhibited by sulfite. *Biochimica et Biophysica Acta (BBA) - Biomembranes*,  
571 1838(7):1809–1816.
- 572 Zhang, Z., Aboulwafa, M., and Saier, M. H. (2014b). Regulation of crp gene expression by the catabolite repres-  
573 sor/activator, cra, in *Escherichia coli*. *Journal of Molecular Microbiology and Biotechnology*, 24(3):135–141.